

# Sulfated and Glucuronidated Conjugates of 3-(4-Hydroxy-3-methoxyphenyl) Propionic Acid Can Promote NO Production by Elevated Ca<sup>2+</sup> Release from the Endoplasmic Reticulum in HUVECs

Tun, Tint Ni Ni

Department of Bioscience and Biotechnology, Faculty of Agriculture, Graduate School of Kyushu University

Yoshino, Susumu

Research Center, Maruzen Pharmaceuticals Co., Ltd.

Kayaki, Hiroyuki

Research Center, Maruzen Pharmaceuticals Co., Ltd.

Kuwahara, Hiroshige

Research Center, Maruzen Pharmaceuticals Co., Ltd.

他

<https://hdl.handle.net/2324/7343015>

---

出版情報 : ACS Omega. 10 (3), pp.2887-2896, 2025-01-16. American Chemical Society (ACS)  
バージョン :  
権利関係 : © 2025 The Authors.

# Sulfated and Glucuronidated Conjugates of 3-(4-Hydroxy-3-methoxyphenyl) Propionic Acid Can Promote NO Production by Elevated $\text{Ca}^{2+}$ Release from the Endoplasmic Reticulum in HUVECs

Tint Ni Ni Tun, Susumu Yoshino, Hiroyuki Kayaki, Hiroshige Kuwahara, and Toshiro Matsui\*

Cite This: *ACS Omega* 2025, 10, 2887–2896

Read Online

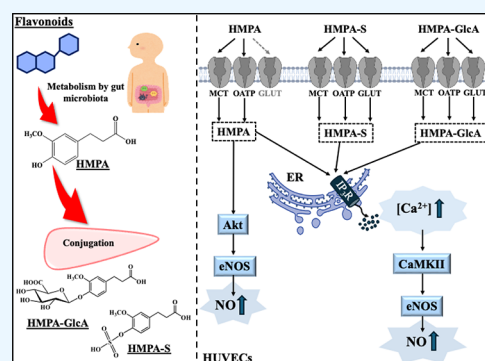
ACCESS |

Metrics &amp; More

Article Recommendations

Supporting Information

**ABSTRACT:** We aimed to clarify whether metabolic conjugates of sulfated and glucuronidated forms have the physiological potential to produce the vasorelaxant nitric oxide (NO) in human umbilical vein endothelial cells (HUVECs), using 3-(4-hydroxy-3-methoxyphenyl) propionic acid (HMPA), a metabolite of dietary flavonoids in the gut. Treatment of HUVECs with sulfated and glucuronidated HMPAs significantly increased NO production and eNOS phosphorylation. A transporter-inhibitor-aided cellular uptake experiment of HMPAs revealed that both conjugates were incorporated into cells via MCT, OATP1A2, and GLUT transporters, whereas intact HMPA was transported via the MCT and OATP1A2 routes. A Fluo-4-probe  $\text{Ca}^{2+}$  assay demonstrated that the incorporated HMPAs significantly increased intracellular  $\text{Ca}^{2+}$  concentration by stimulating the  $\text{IP}_3\text{R}$  of the endoplasmic reticulum in the CaMKII/eNOS signaling cascade. In conclusion, to our knowledge, this study provides the first evidence that sulfated and glucuronidated forms of HMPAs may stimulate NO production in HUVECs.



## 1. INTRODUCTION

3-(4-Hydroxy-3-methoxyphenyl) propionic acid (HMPA) is a metabolite produced by the gut microbiota after ingestion of a polyphenol (or flavonoid)-rich diet.<sup>1–4</sup> In a previous study using Sprague–Dawley (SD) rats, we demonstrated the characteristic pharmacokinetic profiles of HMPA, in which the intact form showed rapid absorption with a  $T_{\text{max}}$  of 15 min and was mainly metabolized into sulfated (HMPA-S) and glucuronidated conjugates (HMPA-GlcA).<sup>5</sup> Our findings highlighted that the orally administered HMPA was efficiently absorbed and accumulated in SD rat bodies (>1.2%), accounting for its conjugated forms. Although there is increasing evidence of the health benefits of HMPA, such as antidiabetic,<sup>6</sup> antiobesity,<sup>7,8</sup> and anticancer effects,<sup>9</sup> the bioactivity of HMPA conjugates in organs remains unclear.

Thus far, it has been reported that a sulfated ferulic acid conjugate (ferulic acid-4-*O*-sulfate) markedly relaxed a phenylephrine-induced contracted aorta in Swiss mice rather than deconjugated ferulic acid, together with *in vivo* blood pressure lowering.<sup>10</sup> Although the *ex vivo* study allowed us to predict that a metabolic conjugate may possess bioactivity in vessels, the underlying mechanisms by which HMPA conjugates enter vascular cells and the manner in which they initiate vasorelaxation-related signaling pathways are still unknown. Influx membrane transporters, such as monocarboxylate transporters (MCTs), organic anion-transporting polypeptides (OATPs), glucose transporters (GLUTs), sodium-dependent glucose transporters (SGLTs), and peptide transporter 1

(PepT1), play a major role in the cellular uptake of most nutrients, including polyphenols, in the circulatory bloodstream.<sup>11</sup> In the endothelial cells used in this study, MCT1/4,<sup>12</sup> OATP1A2,<sup>13</sup> and GLUT1/3<sup>14,15</sup> were highly expressed in human umbilical vein endothelial cells (HUVECs) compared to their other isoforms/subtypes. According to our previous study, administration of HMPA in SD rats (10 mg/kg) led to a significant accumulation of metabolized HMPAs (HMPA-S and -GlcA) in circulating diverse organs. The total amount of conjugated HMPAs accumulated in thoracic aorta (area under the curve,  $\text{AUC}_{0-6\text{ h}}$ : HMPA-S, 0.62 nmol·h/g-tissue; HMPA-GlcA, 0.03 nmol·h/g-tissue) was compatible with intact HMPA (0.92 nmol·h/g-tissue), except for the huge accumulation in the liver and kidneys.<sup>5</sup> The critical finding on the significant accumulation of both HMPA conjugates in the aorta, as well as the reported vasorelaxation effect of sulfated ferulic acid,<sup>10</sup> allowed us to investigate the impact of HMPA conjugates on regulating vessel function including nitric oxide (NO) production and explore the underlying mechanisms involved. NO derived from the endothelium, synthesized by endothelial NO synthase (eNOS), is a strong vasorelaxant

Received: October 2, 2024

Revised: December 22, 2024

Accepted: January 8, 2025

Published: January 16, 2025



signaling molecule that plays a key role in maintaining balanced endothelial function. Endothelial dysfunction, characterized by decreased eNOS activation and reduced NO synthesis, can contribute to the development of various diseases, such as cardiovascular, andrological and kidney disorders, etc.<sup>16,17</sup>

Thus, in the present study, we focused on the vasoactive effect and mechanism of action of conjugated forms of HMPA using HUVECs in terms of (1) intra- or extracellular events and (2) activation pathway(s) of the vasoactive signaling cascade.<sup>18–20</sup>

## 2. MATERIALS AND METHODS

**2.1. Chemicals and Reagents.** HUVECs were obtained from Lonza Japan Ltd. (C2519A, HUVEC-umbilical vein; Lot, 22TL046664, Tokyo, Japan). HMPA (1135-23-5; Lot, F3CCG-GH) was purchased from Tokyo Chemical Industry Co. Ltd. (Tokyo, Japan). Dihydroferulic acid 4-*O*-sulfate sodium salt (HMPA-S, D448915; Lot, 2-QQS-111-2) and dihydroferulic acid 4-*O*- $\beta$ -glucuronide (HMPA-GlcA, D448315; Lot, 2-TRJ-66-2) were purchased from Toronto Research Chemicals, Inc. (North York, ON, Canada). Cytochalasin B, an inhibitor of class I glucose transporters<sup>21</sup> (030–17551; Lot, WTH3813), and KN-62, a Ca<sup>2+</sup>/calmodulin-dependent kinase II (CaMKII) inhibitor (114-0063; Lot, PDK5579), were purchased from Fujifilm Wako Pure Chemicals Co. (Tokyo, Japan). Naringenin, an organic anion transporting polypeptide (OATP1A2) inhibitor<sup>22,23</sup> (102430; Lot, 9784K), was purchased from MP Biomedicals (Santa Ana, California, USA).  $\alpha$ -Cyano-4-hydroxycinnamic acid, a non-specific inhibitor of monocarboxylate transporters<sup>24</sup> ( $\alpha$ -CHCA, C2020; Lot, MKBV1199 V), and 3,4-dimethoxycinnamic acid as an internal standard (IS) (DMCA, D133809; Lot, TBC3700 V) were purchased from Sigma-Aldrich Co. (St. Louis, MO, USA). 2-Aminoethyl diphenylborinate (2-APB, HY-W009724; Lot, S8548), a specific inhibitor of inositol 1,4,5-triphosphate receptor (IP<sub>3</sub>R) in the endoplasmic reticulum (ER), was purchased from Cosmo Bio Co., Ltd. (Tokyo, Japan). Dantrolene sodium (DAN, S5478; Lot, S547802), a specific inhibitor of calcium release from the ER via ryanodine receptor channels (RyR), was purchased from Selleck Chemicals (Houston, TX, USA). The NO<sub>2</sub>/NO<sub>3</sub> assay kit-FX (fluorometric 2,3-diaminonaphthalene kit, NK08; Lot, VK572), a calcium kit II-Fluo 4 (CS22; Lot, WQ118), and a cell counting kit-8 (347–07621; Lot, WC003) were purchased from Dojindo Molecular Technologies (Kumamoto, Japan). Primary antibodies against endothelial NO synthase (eNOS, 32027S; Lot, 5), p-eNOS (Ser1177) (9517S; Lot, 14), serine/threonine kinase (Akt, 9272S; Lot, 28), and p-Akt (Ser473) (9271S; Lot, 15) were purchased from Cell Signaling Technology (Danvers, MA, USA). Water, acetonitrile (ACN), and formic acid (FA) of mass spectrometry (MS) grade were purchased from Merck (Darmstadt, Germany). All other chemicals were of analytical grade and were used without further purification.

**2.2. Cell Culture.** HUVECs were cultured in EGM-2 medium (CC-3162, Lonza Co., Basel, Switzerland) using a Bullet kit containing growth factors (bovine brain extract, ascorbic acid, hydrocortisone, human epidermal growth factor, fetal bovine serum, and gentamicin/amphotericin B) (CC-4176, Lonza Co.). The cells were incubated at 37 °C in a humidified atmosphere (5% CO<sub>2</sub>/95% O<sub>2</sub>), the medium was refreshed the next day, and the cells were conditioned until

80–90% confluence was reached within 4–5 days. Cells at passages of 4–6 were used for all experiments.

**2.3. NO Measurement.** NO measurement was performed using an NO<sub>2</sub>/NO<sub>3</sub> assay kit-FX, according to a previous report, with slight modifications.<sup>25</sup> Briefly, HUVECs at a density of  $3 \times 10^4$  cells/well were seeded in a 48-well plate and incubated in EGM-2 medium for 24 h. Before the samples were added, the cells were washed twice with warmed phosphate-buffered saline (PBS). The cells were then treated with a freshly prepared sample (HMPA, HMPA-S, or HMPA-GlcA at 0.01–1  $\mu$ M) dissolved in EBM-2 medium (1–4 h). After incubation, the collected medium was centrifuged at 1000 g for 15 min, and the amount of NO present in the supernatant NO<sub>2</sub> was measured at excitation and emission wavelengths of 360 and 455 nm, respectively, using a Victor NIVO multimode plate reader (PerkinElmer, Waltham, MA, USA). The level of NO production is expressed as a percentage of the relative fluorescence intensity of the control. In the control group, background fluorescence from the EBM-2 medium was subtracted to eliminate any interference from the medium.

**2.4. Uptake Experiments of HMPAs into HUVECs.** Uptake experiments were performed to study the absorption of HMPAs by HUVECs according to the protocols outlined in previous reports, with minor modifications.<sup>26–28</sup> HUVECs were seeded at a density of  $2 \times 10^5$  cells/well in 6-well plates. After 24 h of incubation, uptake experiments were performed using an incubation medium (phenol red-free EBM-2) (CC-3129, Lonza Co.). After the medium was removed by washing twice with 1.5 mL of fresh medium, the cells were incubated with a medium containing a target (10  $\mu$ M HMPA, HMPA-S, or HMPA-GlcA) for 1 h. Transport route experiments to study absorption of HMPAs into HUVECs were performed using transport inhibitors, and the cells were pretreated with 2 mM  $\alpha$ -CHCA (MCT inhibitor), 100  $\mu$ M naringenin (OATP inhibitor), or 50  $\mu$ M cytochalasin B (GLUT inhibitor) for 30 min before addition of the sample. After the incubation period, uptake was stopped by washing three times with ice-cold phenol red-free EBM-2 medium, and cells were lysed with ice-cold radioimmunoprecipitation assay (RIPA) buffer (150 mM NaCl, 0.5% sodium deoxycholate, 0.1% SDS, 1.0% NP-40, and 50 mM Tris-HCl, pH 8.0) containing 1% PhosSTOP (04906845001; Lot, 71771300, Roche, Indianapolis, IN, USA) and 1% protease inhibitor cocktail (25955–24; Lot, L3H3771, Nacalai Tesque Co., Kyoto, Japan) for 15 min. To determine the incorporated HMPAs using liquid chromatography–quadrupole time-of-flight mass spectrometry (LC-qTOF/MS), 3,4-dimethoxycinnamic acid (DMCA, final concentration of 1.0 nmol/mL) was added as an internal standard (IS) to the RIPA buffer. After harvesting the cells by scraping, the lysates were homogenized for 30 s (twice) at 20,000 rpm at 4 °C with a Polytron homogenizer (Kinematica AG, Luzern, Switzerland) and centrifuged at 14,000 g for 20 min at 4 °C to obtain the supernatant. Protein concentration in the supernatant was determined by using a Pierce BCA Protein Assay Kit (Thermo Fisher Scientific, Inc., Waltham, MA, USA) with bovine serum albumin as a standard.

The supernatant was ultrafiltered using a 0.5 mL Amicon Ultra-15 centrifugal filter (cutoff, 3 K) (Merck Millipore, Carrigtwohill, Ireland) at 14,000 g for 30 min at 4 °C. The resulting filtrate was subjected into LC-qTOF/MS. The concentration of each HMPA was quantified using an IS-aided calibration curve in the range of 0.005–5 nmol/mL. The

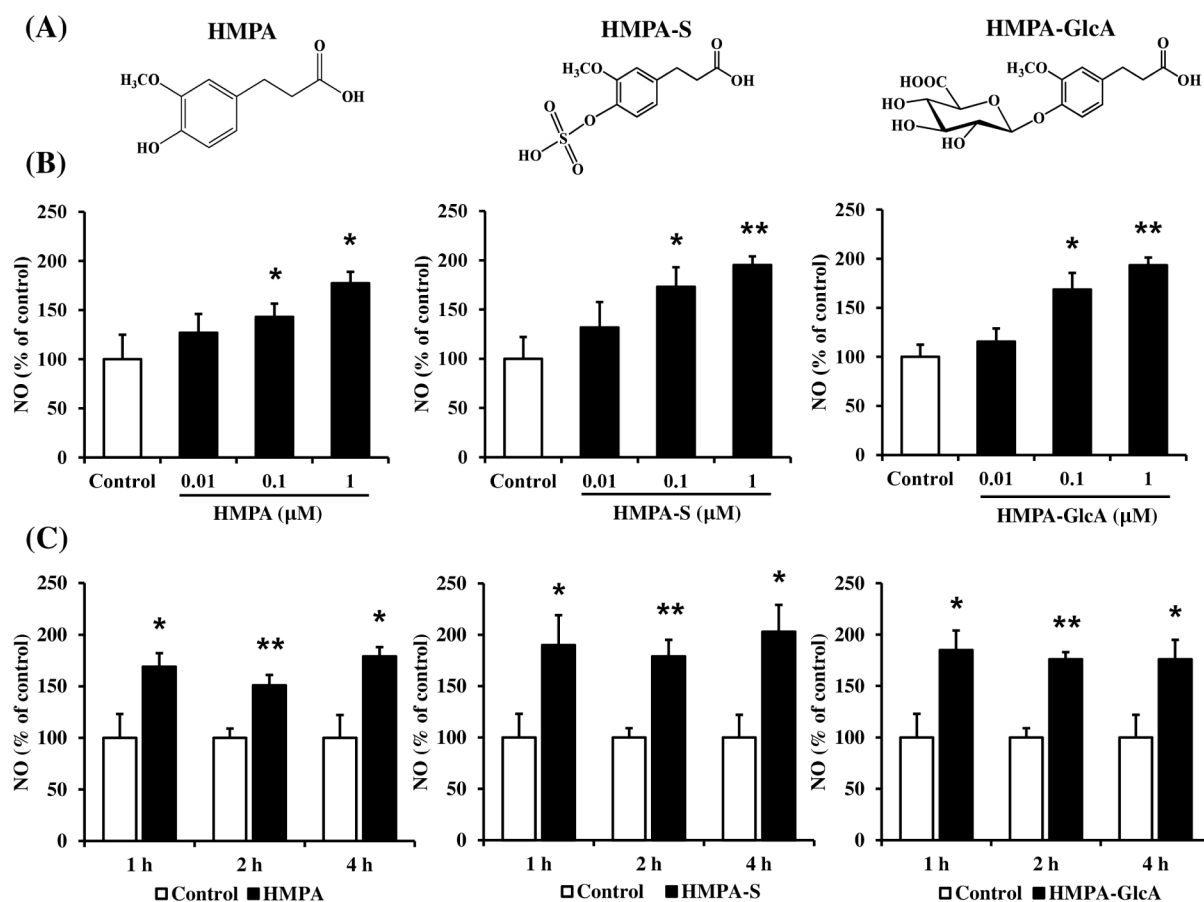


**Figure 1.** Effects of HMPA, HMPA-S, and HMPA-GlcA on NO production in HUVECs. (A) Chemical structures of HMPA, HMPA-S, and HMPA-GlcA. (B) Concentration dependency experiment in 1 h-treated HUVECs: 0.01, 0.1, and 1  $\mu$ M HMPA, HMPA-S, and HMPA-GlcA. (C) Incubation-time dependency experiment in HUVECs treated with 1  $\mu$ M HMPA, HMPA-S, and HMPA-GlcA: 1, 2, and 4 h of incubation time. NO production in HUVECs was assayed by an NO assay-FX kit. Values are expressed as mean  $\pm$  SEM ( $n = 4$  or 6). Significant differences between groups were analyzed by one-way ANOVA, followed by Dunnett's  $t$ -test (B) or Student's  $t$ -test (C) at \*  $p < 0.05$ , \*\*  $p < 0.01$ , vs. control.

linearity and limits of each compound were as follows: HMPA,  $y = 1.6574x - 0.008$ ,  $R^2 = 0.9998$ ; limit of detection [LOD], 0.005 nmol/mL; HMPA-S,  $y = 8.7734x + 0.0186$ ;  $R^2 = 0.9989$ ; LOD, 0.001 nmol/mL; HMPA-GlcA,  $y = 3.8684x + 0.1486$ ,  $R^2 = 0.9974$ ; LOD, 0.005 nmol/mL, where  $x$  is the concentration of the target (nmol/mL) and  $y$  is the ratio of peak areas of the target and DMCA (IS). The amount of uptake by HUVECs was calculated as the amount of HMPA, HMPA-S, or HMPA-GlcA per milligram of protein.

**2.5. Intracellular  $\text{Ca}^{2+}$  Measurement.** The intracellular  $\text{Ca}^{2+}$  concentration ( $[\text{Ca}^{2+}]_i$ ) was assayed using a calcium kit II-Fluo 4, according to the manufacturer's protocol. Briefly, HUVECs were seeded at  $1.5 \times 10^4$  cells/well in a 96-well plate and incubated in EGM-2 medium for 24 h. After incubation, a loading buffer (100  $\mu$ L) containing Fluo 4-AM in Hank's HEPES buffer plus 5% pluronic F-127 and 250 mM probenecid was added to each well and incubated in the dark for 1 h at 37  $^\circ\text{C}$ . For inhibitor experiments using 30  $\mu$ M 2-APB or 10  $\mu$ M dantrolene, each well was preincubated with inhibitor solution for 30 min before adding the loading buffer.  $[\text{Ca}^{2+}]_i$  was detected at an excitation wavelength of 485 nm and emission wavelength of 525 nm using a Flex Station 3 multimode microplate reader (Molecular Devices, Sunnyvale, CA, USA). After recording the baseline fluorescence ( $F_0$ ) signal for 30 s, a sample solution (40  $\mu$ L of 1  $\mu$ M HMPA, HMPA-S, or HMPA-GlcA-containing Hank's HEPES buffer)

was added to each well through a multichannel pipet included as a part of the fluidics module of Flex Station 3. The maximum fluorescence ( $F_{\text{max}}$ ) signal was recorded for an additional 60 s. Change in relative Fluo-4 fluorescence or change in  $[\text{Ca}^{2+}]_i$  was expressed as  $\Delta F = (F_{\text{max}} - F_0)$ .

**2.6. LC-qTOF/MS Analysis.** LC separation was conducted with an Agilent 1200 Series Gradient HPLC system (Agilent Technologies, Waldbronn, Germany) equipped with a COSMOSIL C18-AR-II column (2.0  $\times$  150 mm, 4.6  $\mu$ m, Nacalai Tesque, Inc.) at 40  $^\circ\text{C}$ . The mobile phase consisted of water (solvent A) and ACN (solvent B), both containing 0.1% FA, with a 20 min linear gradient from 0% to 100% solvent B at a flow rate of 0.2 mL/min. The qTOF/MS analysis was carried out using a Compact qTOF/MS (Bruker Daltonics, Bremen, Germany) system operated in negative electrospray-ionization (ESI) mode. Mass spectral data were collected in the range of 100–1000  $m/z$ . HMPA, HMPA-S, HMPA-GlcA, and DMCA (IS) were detected based on their  $[\text{M}-\text{H}]^-$  of 195.0653, 275.0220, 371.0973, and 207.0657  $m/z$ , respectively (width of  $m/z$ ,  $\pm 0.01$ ). The MS conditions were as follows: nebulizer pressure, 2.0 bar; dry gas, nitrogen; dry gas flow, 8.0 L/min; drying temperature, 200  $^\circ\text{C}$ ; and capillary voltage, 4500 V. A calibration solution of 10 mM sodium formate in 50% ACN was injected into the MS system at the beginning of each run. The data were analyzed and acquired by using Bruker Compass Data Analysis 4.3 software.

**2.7. Measurement of Protein Expression.** The protein expression levels of p-eNOS, eNOS, p-Akt, and Akt in HUVECs were measured using a capillary electrophoretic-based immunoassay Wes instrument (ProteinSimple Co., San Jose, CA, USA) with a 12–230 kDa separation module ( $8 \times 25$  mm capillary cartridge; ProteinSimple Co.). Briefly, HUVECs were seeded at a density of  $2 \times 10^5$  cells/well in a 6-well plate and treated with HMPA, HMPA-S, and HMPA-GlcA at  $1 \mu\text{M}$  for 1 h at  $37^\circ\text{C}$ . Cell lysate preparation was performed as described in Section 2.4. For the Wes measurement, the supernatant of the cell lysate was combined with a  $0.1 \times$  sample diluent buffer and a  $5 \times$  fluorescent master mix denaturing buffer (ProteinSimple Co.) to obtain a  $0.4 \mu\text{g}/\mu\text{L}$  loading concentration, followed by denaturation at  $95^\circ\text{C}$  for 5 min. Primary antibodies for p-Akt, Akt, and p-eNOS were diluted to a 1:50 ratio, and primary antibody for eNOS was diluted to a 1:10 ratio. Samples, biotinylated ladder (marker), blocking reagent, primary antibodies, horseradish peroxidase-conjugated antirabbit secondary antibody, and a chemiluminescent substrate were dispensed into a microplate and subjected to Wes-automated capillary electrophoresis, followed by automated immunodetection. The resulting chemiluminescent signal was displayed as a virtual blot-like image, and an electropherogram was generated based on molecular weights using Compass software (ProteinSimple Co.). Protein expression of p-eNOS/eNOS and p-Akt/Akt was normalized to the electropherogram peak area of the total protein applied to each lane, and the data were expressed as ratios against the control.

**2.8. Statistical Analysis.** Results are expressed as the mean  $\pm$  standard error of the mean (SEM). Statistical differences between multiple groups were evaluated using a one-factor analysis of variance (ANOVA), followed by Dunnett's or Tukey's *t*-test for *post hoc* analysis. An unpaired two-tailed Student's *t*-test was used to compare values between two groups. Statistical significance was set at  $p < 0.05$ . All analyses were performed using GraphPad Prism ver. 5.0 (La Jolla, CA, USA).

### 3. RESULTS

**3.1. NO Production Ability of HMPA Conjugates in HUVECs.** Based on previous findings on local accumulation of sulfated, glucuronidated HMPA, and intact HMPA in the rat aorta<sup>5</sup> and NO production by HMPA,<sup>29</sup> we conducted cell-based experiments to evaluate NO production, a key indicator of vasorelaxation in HUVECs. These experiments were conducted using intact HMPA and its HMPA-S and HMPA-GlcA conjugates (Figure 1A). As shown in Figure 1B, both HMPA conjugates exhibited NO production ability in a concentration ( $0.01$ – $1 \mu\text{M}$ )-dependent manner, similar to intact HMPA. Considering the effect of incubation time (1–4 h) on NO production by different forms of HMPA (Figure 1C), further experiments were carried out by using  $1 \mu\text{M}$  1 h-treated HUVECs (NO production of intact HMPA,  $174 \pm 17\%$ ,  $p < 0.05$ ; HMPA-S,  $195 \pm 22\%$ ,  $p < 0.01$ ; HMPA-GlcA,  $184 \pm 8\%$ ,  $p < 0.01$ ).

**3.2. Effect of HMPA Conjugates on eNOS Expression in HUVECs.** To confirm that HMPA conjugates had the ability to promote NO production, eNOS activation by conjugates was examined in  $1 \mu\text{M}$  1 h-treated HUVECs. Wes analysis revealed that HMPA-S, HMPA-GlcA, and intact HMPA significantly induced phosphorylation of eNOS (Figure 2), indicating that even a conjugated S- or GlcA-form of HMPA

may facilitate physiological action by activating eNOS in HUVECs.

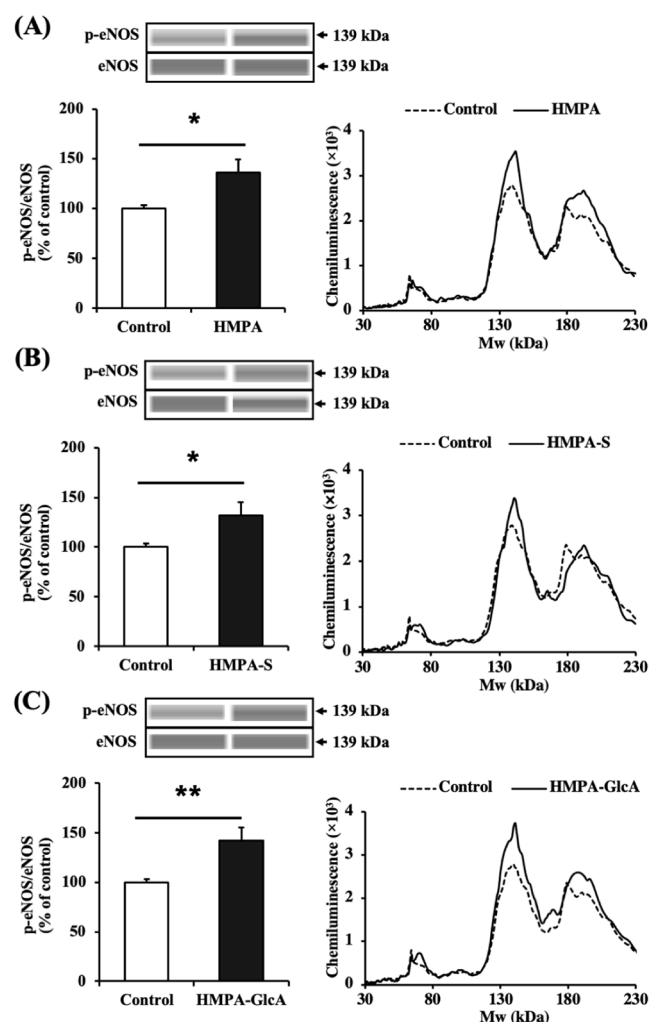


**Figure 2.** Effects of (A) HMPA, (B) HMPA-S, and (C) HMPA-GlcA on eNOS phosphorylation in  $1 \mu\text{M}$  1 h-treated HUVECs. eNOS protein expression analyzed by the Wes analysis was normalized by the electropherogram peak area of the applied total protein in each lane. The chemiluminescence signal is displayed as a virtual blot-like image, and an electropherogram was generated based on the molecular weight. Values are expressed as mean  $\pm$  SEM ( $n = 4$  or  $6$ ). Statistical analysis between two groups was performed by Student's *t*-test, \*  $p < 0.05$ , \*\*  $p < 0.01$  vs. control.

**3.3. Uptake Behavior of HMPA Conjugates into HUVECs.** Prior to elucidating the mechanism of activation of the eNOS/NO signaling pathway by the HMPA conjugates, we attempted to confirm the incorporation of HMPA conjugates into the cells. As shown in Figure S2, MS chromatograms revealed that intact HMPA, as well as its S- and GlcA-conjugates, were incorporated into cells; the amount of incorporated intact HMPA, HMPA-S, and HMPA-GlcA in the cell lysate from  $1 \mu\text{M}$  1 h-treated HUVECs was quantified by IS-aided LC-qTOF/MS to be  $0.120 \pm 0.013$  nmol/mg-protein,  $0.033 \pm 0.005$  nmol/mg-protein, and  $0.013 \pm 0.002$  nmol/mg-protein, respectively. HMPA uptake experiments were performed by focusing on their transport routes using inhibitors targeting the MCT, OATP, and GLUT transporters. MCT inhibitor  $\alpha$ -CHCA and OATP1A2 inhibitor naringenin

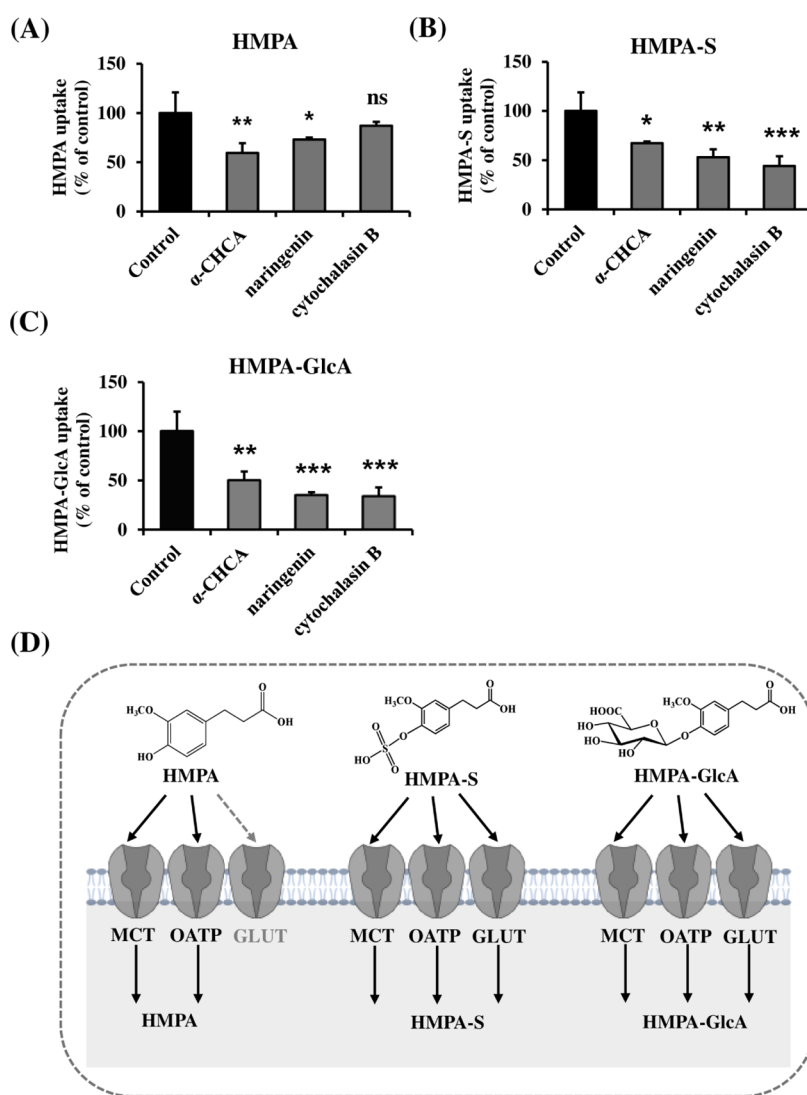


**Figure 3.** Effects of transport inhibitors on uptake of HMPA and its conjugates by 10  $\mu$ M 1 h-treated HUVECs. Uptake of (A) HMPA, (B) HMPA-S, and (C) HMPA-GlcA in the presence or absence of 2 mM  $\alpha$ -CHCA, 100  $\mu$ M naringenin, or 50  $\mu$ M cytochalasin B in the lysate of HUVECs. HUVECs were pretreated with or without the inhibitors for 30 min, then exposed to 1  $\mu$ M of each sample (HMPA, HMPA-S, and HMPA-GlcA) for 1 h at 37  $^{\circ}$ C, respectively. (D) Summary of uptake routes of HMPAs in HUVECs. Data are shown as percentage of control (uptake without inhibitor) and expressed as mean  $\pm$  SEM ( $n = 3$ ). Statistical analysis was performed by one-way ANOVA, followed by Dunnett's  $t$ -test, \*  $p < 0.05$ , \*\*  $p < 0.01$ , \*\*\*  $p < 0.001$  vs control (uptake without inhibitor); n.s. no significance at  $p > 0.05$ .

significantly reduced the uptake of intact HMPA, whereas no reduction was observed with cytochalasin B (GLUT inhibitor) (Figure 3A). In contrast, the uptake of both HMPA-S and HMPA-GlcA conjugates was significantly affected by all of the inhibitors used in this study (Figure 3B,C). Taken together, it was found that sulfated and glucuronidated forms of HMPA could be incorporated into HUVECs, possibly through the carrier-mediated routes of MCTs, OATP, and GLUTs transporters, although intact HMPA transport was restricted to the MCTs and OATP routes (Figure 3D).

**3.4. Effect of HMPA Conjugates on Akt Phosphorylation Levels in HUVECs.** To elucidate the mechanism involved in eNOS activation and NO production by HMPA conjugates, we first examined the involvement of phosphatidylinositol-3 kinase (PI3K) and the downstream serine/threonine kinase Akt by assessing the phosphorylation levels of the Akt protein using Wes analysis. As shown in Figure 4, intact HMPA significantly increased Akt phosphorylation compared to the control group. However, HMPA conjugates

did not exhibit this effect. These findings prompted us to further elucidate the mechanisms involved in eNOS activation and NO production by HMPA conjugates via  $\text{Ca}^{2+}$ -dependent signaling pathways in endothelial cells.

**3.5. Effect of HMPA Conjugates on Intracellular  $\text{Ca}^{2+}$  Release in HUVECs.** To elucidate the activation mechanism of the eNOS/NO signaling pathway by HMPA conjugates incorporated by HUVECs, changes in  $[\text{Ca}^{2+}]_i$  in HUVECs exposed to 1  $\mu$ M HMPA, HMPA-S, or HMPA-GlcA for 90 s were monitored using a Fluo-4-aided Flex Station 3 microplate reader, as elevated intracellular  $\text{Ca}^{2+}$  triggers eNOS phosphorylation at Ser1177.<sup>30</sup> As depicted in Figure 5, the addition of each HMPA caused a rapid and similar increase in  $[\text{Ca}^{2+}]_i$ , compared to the control (Hank's HEPES buffer) group, suggesting that the conjugates as well as intact HMPA stimulated increased intracellular  $\text{Ca}^{2+}$  levels after their incorporation into cells (Figure 5D). To clarify the mechanism underlying the  $[\text{Ca}^{2+}]_i$  increase by the conjugates, the effect of HMPAs on  $\text{Ca}^{2+}$  release from the ER serving as a main  $\text{Ca}^{2+}$

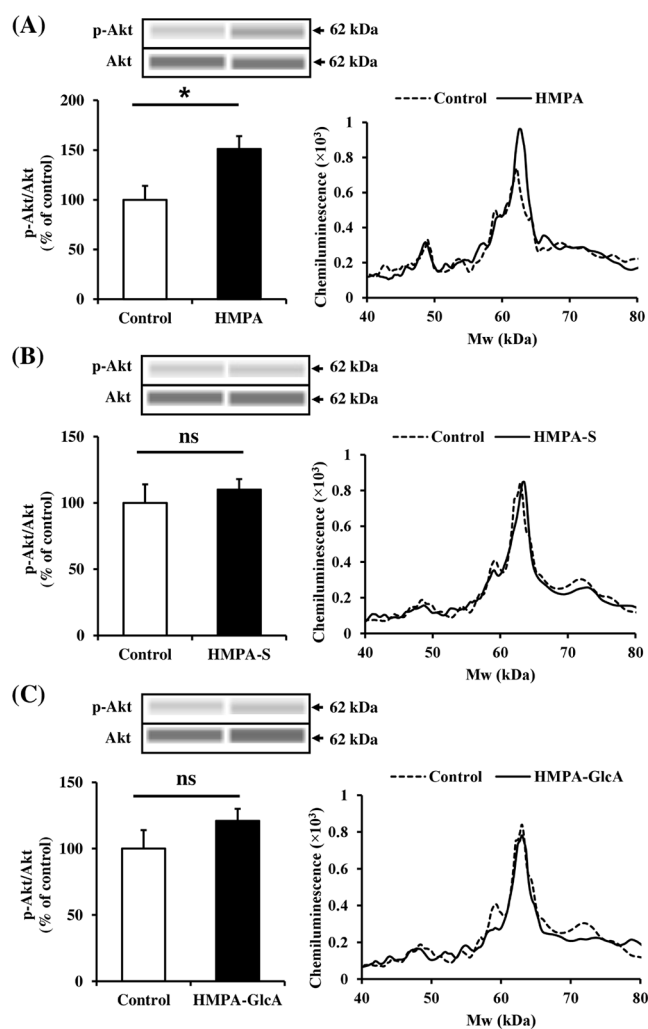


**Figure 4.** Effects of (A) HMPA, (B) HMPA-S, and (C) HMPA-GlcA on phosphorylation levels of Akt in HUVECs. HUVECs were treated with 1  $\mu$ M HMPA conjugates for 1 h. Akt protein expression analyzed by the Wes analysis was normalized by the electropherogram peak area of the applied total protein in each lane. The chemiluminescence signal is displayed as a virtual blot-like image, and an electropherogram was generated based on the molecular weight. Values are expressed as mean  $\pm$  SEM ( $n = 4$  or 6). Statistical analysis between two groups was performed by Student's  $t$ -test, \*  $p < 0.05$  vs control; n.s. no significance at  $p > 0.05$ .

storage compartment<sup>31</sup> was investigated using inhibitors of IP<sub>3</sub>R and RyR Ca<sup>2+</sup> channels.<sup>32</sup> As shown in the fluorescence profiles inserted in Figure 5D, 2-APB, an IP<sub>3</sub>R inhibitor, greatly suppressed the increase in [Ca<sup>2+</sup>]<sub>i</sub> induced by each HMPA, while no changes in [Ca<sup>2+</sup>]<sub>i</sub> were observed in the presence of dantrolene, an RyR inhibitor (Figure S4). These findings strongly suggest that HMPA-S, HMPA-GlcA, and intact HMPA play an intracellular role in stimulating IP<sub>3</sub>R, but not RyR. In addition, the present result, indicating that all of the HMPAs were IP<sub>3</sub>R stimulators, led us to speculate on the importance of the HMPA moiety (or no involvement of the groups attached to the HMPA moiety) in exerting this effect. However, further studies regarding *in silico* simulation analysis of HMPA with IP<sub>3</sub>R protein are needed to clarify the intermolecular interaction of sulfated and glucuronidated HMPA forms with the receptor.<sup>33</sup>

In the axis of Ca<sup>2+</sup>-eNOS/NO signaling cascade, Ca<sup>2+</sup>/calmodulin-dependent kinases, including CaMKII and CaMK kinase  $\beta$  (CaMKK $\beta$ ), are associated with eNOS activation.<sup>34</sup> As shown in Figure 6, CaMKII inhibition by the KN-62 inhibitor significantly reduced the promotion of NO production by HMPAs. Although the involvement of the CaMKK $\beta$  pathway in promoting NO production by the conjugates cannot be excluded, the NO production potential of intact and conjugated HMPAs was induced by activation of CaMKII/eNOS signaling by triggering elevated [Ca<sup>2+</sup>]<sub>i</sub> via IP<sub>3</sub>R stimulation within the present study (Figure 7).

#### 4. DISCUSSION

To date, there have been few studies on the bioactivity of metabolic conjugates of dietary polyphenols, such as sulfated and glucuronidated forms. This is because (1) conjugated standards are less available and (2) quantitative evaluation of polyphenol conjugates in organ tissues has not been performed. Van Rymenant et al. claimed that sulfated conjugated forms such as sulfated ferulic acid may exhibit vasorelaxant effect when added to a constricted SD rat aorta.<sup>10</sup> Another study showed that glucuronidated and sulfated flavonoid metabolites (not their unmetabolized precursors) showed potent anti-inflammatory effects in human endothelial cells.<sup>35</sup> This study also supported the hypothesis that metabolic conjugation may not alter the physiological potential of intact polyphenols, although the underlying mechanism(s) of the conjugated forms remained unclear. In the present study, we investigated the physiological potential of monosulfated or monoglucuronidated forms of HMPA, each bearing a monohydroxyl group, and their beneficial effects on the cardiovascular system by assessing the levels of NO, a potent vasorelaxant signaling molecule, and elucidated the underlying mechanism of NO production from monosulfated or monoglucuronidated forms of HMPA in HUVECs. The investigation was based on the evidence of local accumulation of HMPA and its conjugates in the aorta tissues after oral HMPA administration in SD rats,<sup>5</sup> and the commercially available standards of monosulfated HMPA (HMPA-S) and monoglucuronidated HMPA (HMPA-GlcA). As summarized in Figure 7, the metabolic conversion of HMPA to sulfated or glucuronidated form did not alter the NO production potential of intact (or preconjugated) HMPA. The mechanism of the HMPA-conjugate-induced NO production in HUVECs was due to the activation of the Ca<sup>2+</sup>-mediated CaMKII/eNOS signaling pathway, triggered by the incorporation of HMPA-S and HMPA-GlcA conjugates into the cells through the MCT/OATP/GLUT routes following an elevated [Ca<sup>2+</sup>]<sub>i</sub> by IP<sub>3</sub>R stimulation.

As mentioned above, sulfation of ferulic acid (ferulic acid-4-O-sulfate) induces vasorelaxation in *ex vivo* vasoconstriction experiments, in which sulfated ferulic acid relaxes the aorta in an NO- or endothelial-independent manner.<sup>10</sup> Moreover, the authors claimed that the sulfated compound activated soluble guanylate cyclase (sGC) following cyclic GMP production in vascular smooth muscle cells, causing hyperpolarization of the cell membrane via an elevated K<sup>+</sup> efflux. In addition, the sulfation of ferulic acid was not presumed to be an interfering factor in intracellular uptake across the vascular endothelial layer; however, the mechanism of sulfated-form-induced sGC activation remains unclear. Recently, Serreli et al. have reported that the sulfated form of isoferulic acid, an isomer of ferulic acid, is a potent NO production enhancer acting on

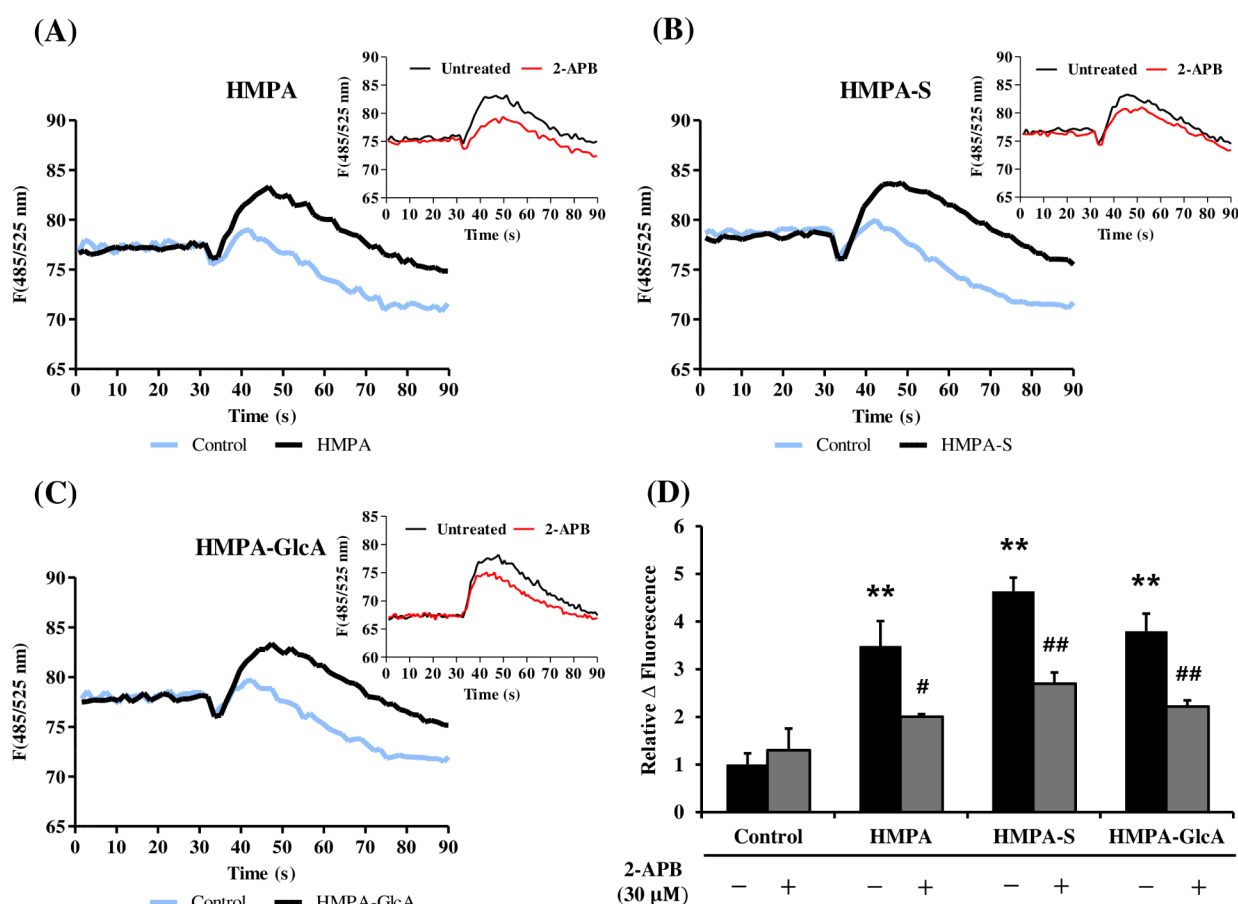


**Figure 5.** Change in intracellular  $\text{Ca}^{2+}$  concentration in HUVECs treated with  $1 \mu\text{M}$  (A) HMPA, (B) HMPA-S, and (C) HMPA-GlcA by Fluo-4 fluorescence assay. HUVECs were loaded with Fluo-4-AM buffer and incubated for 1 h. After measuring a baseline fluorescence of Fluo-4-AM-loaded HUVECs for 30 s, each HMPA was added, and the fluorescence intensity was monitored at 485 nm/525 nm. (D) Relative  $\Delta$  fluorescence of HMPAs against that of control, in the presence or absence of  $30 \mu\text{M}$  2-APB for 30 min before Fluo-4-AM loading were evaluated. Values are expressed as mean  $\pm$  SEM ( $n = 6$  or 8). Statistical differences between groups in the absence of 2-APB were evaluated using Tukey-Kramer's  $t$ -test,  $**p < 0.01$  vs control. Statistical analysis between two groups in the presence or absence of 2-APB was performed by Student's  $t$ -test, #  $p < 0.05$ , ##  $p < 0.01$ .

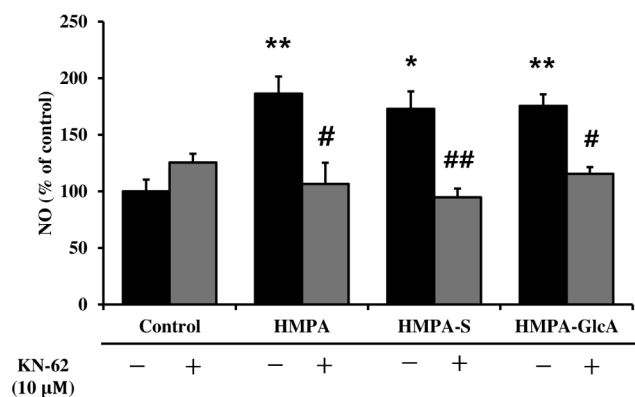


**Figure 6.** Effects of HMPA, HMPA-S, and HMPA-GlcA on NO production in the presence of KN-62 (CaMKII inhibitor,  $10 \mu\text{M}$ ) in  $1 \mu\text{M}$  1 h-treated HUVECs. Effect of KN-62 (CaMKII inhibitor,  $10 \mu\text{M}$ ) on NO production in  $1 \mu\text{M}$  1 h-treated HUVECs with HMPAs was evaluated. HUVECs were pretreated with  $10 \mu\text{M}$  KN-62 for 30 min before addition of HMPAs. Values are expressed as mean  $\pm$  SEM ( $n = 4$ – $6$ ). Statistical differences were evaluated using Dunnett's  $t$ -test. \*  $p < 0.05$ , \*\*  $p < 0.01$  vs control. Statistical analysis between two groups in the presence or absence of KN-62 was performed by Student's  $t$ -test, #  $p < 0.05$ , ##  $p < 0.01$ .

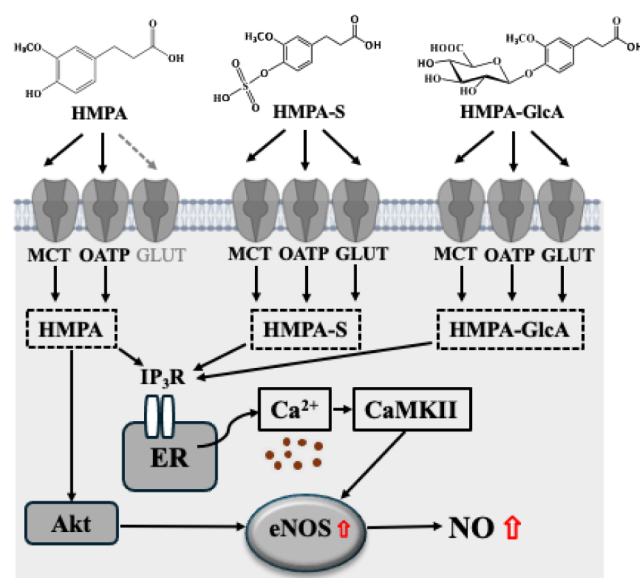


**Figure 7.** Schematic representation of HMPA-stimulated signaling pathway in HUVECs.

endothelial cells,<sup>29</sup> which is in good agreement with our results for sulfated HMPA (Figure 1). The different sites of action between sulfated compounds may be related to differences in the phenolic moiety but not the sulfate group, presumably resulting in different cellular uptake and/or events. The authors also provided useful information on the conjugated form, in which the glucuronidated form of ferulic acid is a bioactive enhancer of NO production. This finding is consistent with the effects observed for glucuronidated HMPA (Figure 1) and flavanol conjugates. Thus, it is likely that the formation of metabolic conjugates, including sulfated and glucuronidated forms, does not reduce the bioactive potentials, such as NO production,<sup>10,29,36</sup> and glucose uptake by promoting GLUT translocation in myotubes.<sup>37</sup>

Despite the observed NO-producing effect of HMPA conjugates on endothelial cells, little is known about the interaction of these conjugates or the mechanism of entry into the cells. In this study, we demonstrated that HMPA conjugates (HMPA-S and HMPA-GlcA) could be incorporated into HUVECs through the MCT, OATP, and/or GLUT routes; however, in the present inhibitor-aided experiments (Figure 3), we could not determine the favorable route(s). In GLUT transport route experiments, cytochalasin B was used as a specific inhibitor against GLUTs; however, we also employed KGA2727, which is an inhibitor of sodium-dependent glucose transporter (SGLT1) to examine the role of SGLT1. The results revealed that the transport behavior of HMPA conjugates is similar to that of GLUTs (data not shown). Although the expression of SGLT1 was negligible in HUVECs compared to that in GLUTs,<sup>38</sup> we concluded that the glucose transporting system is preferentially involved in the uptake of the conjugates, mainly via the GLUT1/3 routes. It has been reported that quercetin<sup>39,40</sup> and resveratrol<sup>41</sup> are transported via OATP routes, whereas ferulic acid is recognized by MCTs in Caco-2 cell monolayers.<sup>42</sup> Different transport routes depending on polyphenols and less study on transporting routes of conjugated forms may lead us to investigate more studies on the molecular properties of conjugated forms. *In silico* studies<sup>33</sup> simulating each target transporter protein are now in progress.

In endothelial cells, eNOS activation and resulting NO production can be amplified by various factors, including shear stress, acetylcholine, bradykinin, and histamine, through both Ca<sup>2+</sup>-dependent and Ca<sup>2+</sup>-independent pathways.<sup>43</sup> Increases in the intracellular Ca<sup>2+</sup> concentration lead to the activation of the calmodulin-binding domain of eNOS and NO production,<sup>44</sup> whereas phosphorylation of eNOS, independent of Ca<sup>2+</sup> concentration, occurs via PI3K and the downstream Ser/Thr kinase Akt.<sup>45</sup> Our results revealed that intact HMPA stimulated NO production via both Akt/eNOS/NO and calcium-dependent signaling pathways (Figures 4 and 5). Meanwhile, HMPA, HMPA-S, and HMPA-GlcA significantly elevated intracellular Ca<sup>2+</sup> levels, which were abolished by IP<sub>3</sub>R and CaMKII inhibitions (Figures 5 and 6). This led us to speculate that the mother skeleton of HMPA plays an intracellular role in activating the IP<sub>3</sub>R-mediated Ca<sup>2+</sup>-dependent CaMKII/eNOS signaling pathway, and an increase in intracellular Ca<sup>2+</sup> is an important pathway for HMPA-S and HMPA-GlcA, leading to eNOS/NO activation.

In conclusion, we demonstrated that the conjugated forms of HMPA-S and HMPA-GlcA promote the production of NO after cellular uptake by HUVECs via carrier-mediated proteins such as MCTs, OATP1A2, and GLUTs, following the IP<sub>3</sub>R-

stimulated Ca<sup>2+</sup>-CaMKII/eNOS signaling pathway. These findings highlight the significance of considering sulfated and glucuronidated conjugates of polyphenols, particularly the gut metabolite HMPA from this study, as a group of physiologically functional candidates with the potential to improve cardiovascular health.

## ■ ASSOCIATED CONTENT

### Data Availability Statement

All data generated or analyzed during this study are included in this article (and its supplementary files).

### Supporting Information

The Supporting Information is available free of charge at <https://pubs.acs.org/doi/10.1021/acsomega.4c09008>.

Uncropped virtual blot-like images of p-eNOS/eNOS expression using the Wes analysis in 1  $\mu$ M 1 h-treated HUVECs with HMPA, HMPA-S, or HMPA-GlcA (Figure S1); LC-qTOF/MS chromatograms of HMPA, HMPA-S, and HMPA-GlcA in the presence or absence of influx transport inhibitors in HUVECs (Figure S2); calibration curves for quantification of HMPA, HMPA-S, and HMPA-GlcA using LC-qTOF/MS (Figure S3); effect of dantrolene (RyR inhibitor, 10  $\mu$ M) on intracellular Ca<sup>2+</sup> levels induced by HMPA, HMPA-S, and HMPA-GlcA (Figure S4); and uncropped virtual blot-like images of p-Akt/Akt expression using the Wes analysis in 1  $\mu$ M 1 h-treated HUVECs with HMPA, HMPA-S, and HMPA-GlcA (Figure S5) (PDF)

## ■ AUTHOR INFORMATION

### Corresponding Author

Toshiro Matsui – Department of Bioscience and Biotechnology, Faculty of Agriculture, Graduate School of Kyushu University, Fukuoka 819-0395, Japan; [orcid.org/0000-0002-9137-8417](https://orcid.org/0000-0002-9137-8417); Email: [tmatsui@agr.kyushu-u.ac.jp](mailto:tmatsui@agr.kyushu-u.ac.jp)

### Authors

Tint Ni Ni Tun – Department of Bioscience and Biotechnology, Faculty of Agriculture, Graduate School of Kyushu University, Fukuoka 819-0395, Japan; [orcid.org/0000-0002-6556-1541](https://orcid.org/0000-0002-6556-1541)

Susumu Yoshino – Research Center, Maruzen Pharmaceuticals Co., Ltd., Fukuyama 729-3102, Japan

Hiroyuki Kayaki – Research Center, Maruzen Pharmaceuticals Co., Ltd., Fukuyama 729-3102, Japan

Hiroshige Kuwahara – Research Center, Maruzen Pharmaceuticals Co., Ltd., Fukuyama 729-3102, Japan

Complete contact information is available at: <https://pubs.acs.org/10.1021/acsomega.4c09008>

### Author Contributions

T.N. performed cell line experiments. T.N. and T.M. analyzed and discussed the results. T.N. wrote the original draft. T.M., S.Y., H.Kay, and H.Kuw reviewed and edited the manuscript. T.M. designed and supervised the study. All the authors have read and approved the final manuscript for publication.

### Notes

The authors declare no competing financial interest.

## ■ ACKNOWLEDGMENTS

This study was partially supported by JSPS KAKENHI [grant number JP21H04863 (T.M.)].

## ABBREVIATIONS

ACN, acetonitrile; CaMKII, Ca<sup>2+</sup>/calmodulin-dependent kinase II; CaMKK $\beta$ , Ca<sup>2+</sup>/calmodulin-dependent kinase kinase  $\beta$ ;  $\alpha$ -CHCA,  $\alpha$ -cyano-4-hydroxycinnamic acid; DMCA, 3,4-dimethoxy cinnamic acid; eNOS, endothelial nitric oxide synthase; ER, endoplasmic reticulum; FA, formic acid; GLUT, glucose transporter; HMPA, 3-(4-hydroxy-3-methoxyphenyl) propionic acid; HMPA-GlcA, glucuronidated HMPA; HMPA-S, sulfated HMPA; HUVEC, human umbilical vein endothelial cell; IP<sub>3</sub>R, inositol 1,4,5-triphosphate receptor; MCT, monocarboxylate transporter; NO, nitric oxide; OATP, organic anion transporting polypeptide; qTOF/MS, quadrupole time-of-flight/mass spectrometry; sGC, soluble guanylate cyclase

## REFERENCES

- (1) Cárdenas-Castro, A. P.; Rochín-Medina, J. J.; Ramírez, K.; Tovar, J.; Sáyago-Ayerdi, S. G. *In vitro* intestinal bioaccessibility and colonic biotransformation of polyphenols from mini bell peppers (*Capsicum annuum* L.). *Plant Foods Hum. Nutr* **2022**, *77* (1), 77–82.
- (2) Roowi, S.; Mullen, W.; Edwards, C. A.; Crozier, A. Yogurt impacts on the excretion of phenolic acids derived from colonic breakdown of orange juice flavanones in humans. *Mol. Nutr. Food Res* **2009**, *53* (S1), S68–S75.
- (3) Pereira-Caro, G.; Borges, G.; Van Der Hooft, J.; Clifford, M. N.; Del Rio, D.; Lean, M. E.; Roberts, S. A.; Kellerhals, M. B.; Crozier, A. Orange juice (poly) phenols are highly bioavailable in humans. *Am. J. Clin. Nutr* **2014**, *100* (5), 1378–1384.
- (4) Bresciani, L.; Angelino, D.; Vivas, E. I.; Kerby, R. L.; García-Viguera, C.; Del Rio, D.; Rey, F. E.; Mena, P. Differential catabolism of an anthocyanin-rich elderberry extract by three gut microbiota bacterial species. *J. Agric. Food Chem* **2020**, *68* (7), 1837–1843.
- (5) Abe, C.; Soma, A.; Tun, T. N. N.; Zhang, Y.; Nishitani, Y.; Kayaki, H.; Kawakami, H.; Matsui, T. Pharmacokinetic profiles of 3-(4-hydroxy-3-methoxyphenyl) propionic acid and its conjugates in Sprague-Dawley rats. *Biosci., Biotechnol., Biochem* **2023**, *87* (5), 516–524.
- (6) Croft, K. D.; Yamashita, Y.; O'Donoghue, H.; Shirasaya, D.; Ward, N. C.; Ashida, H. Screening plant derived dietary phenolic compounds for bioactivity related to cardiovascular diseases. *Fitoterapia* **2018**, *126*, 22–28.
- (7) Ohue-Kitano, R.; Taira, S.; Watanabe, K.; Masujima, Y.; Kuboshima, T.; Miyamoto, J.; Nishitani, Y.; Kawakami, H.; Kuwahara, H.; Kimura, I. 3-(4-Hydroxy-3-methoxyphenyl) propionic acid produced from 4-hydroxy-3-methoxycinnamic acid by gut microbiota improves host metabolic condition in diet-induced obese mice. *Nutrients* **2019**, *11* (5), 1036.
- (8) Ohue-Kitano, R.; Masujima, Y.; Nishikawa, S.; Iwasa, M.; Nishitani, Y.; Kawakami, H.; Kuwahara, H.; Kimura, I. 3-(4-Hydroxy-3-methoxyphenyl) propionic acid contributes to improved hepatic lipid metabolism via GPR41. *Sci. Rep* **2023**, *13* (1), 21246.
- (9) Martini, S.; Conte, A.; Tagliazucchi, D. Antiproliferative activity and cell metabolism of hydroxycinnamic acids in human colon adenocarcinoma cell lines. *J. Agric. Food Chem* **2019**, *67* (14), 3919–3931.
- (10) Van Rymenant, E.; Van Camp, J.; Pauwels, B.; Boydens, C.; Daele, L. V.; Beerens, K.; Brouckaert, P.; Smagghe, G.; Kerimi, A.; Williamson, G.; Grootaert, C. Ferulic acid-4-*O*-sulfate rather than ferulic acid relaxes arteries and lowers blood pressure in mice. *J. Nutr. Biochem* **2017**, *44*, 44–51.
- (11) Matsui, T. Polyphenols-absorption, and occurrence in the body system. *Food Sci. Technol. Res* **2022**, *28* (1), 13–33.
- (12) Sonveaux, P.; Copetti, T.; De Saedeleer, C. J.; Vegran, F.; Verrax, J.; Kennedy, K. M.; Moon, E. J.; Dhup, S.; Danhier, P.; Frérart, F.; Gallez, B.; Deutsch, E. Targeting the lactate transporter MCT1 in endothelial cells inhibits lactate-induced HIF-1 activation and tumor angiogenesis. *PLoS One* **2012**, *7* (3), No. e33418.
- (13) Ronaldson, P. T.; Brzica, H.; Abdullahi, W.; Reilly, B. G.; Davis, T. P. Transport properties of statins by organic anion transporting polypeptide 1A2 and regulation by transforming growth factor- $\beta$  signaling in human endothelial cells. *J. Pharmacol. Exp. Ther* **2021**, *376* (2), 148–160.
- (14) Wu, W. Z.; Bai, Y. P. Endothelial GLUTs and vascular biology. *Biomed. Pharmacother* **2023**, *158*, 114151.
- (15) Mamun, A. A.; Hayashi, H.; Yamamura, A.; Nayeem, M. J.; Sato, M. Hypoxia induces the translocation of glucose transporter 1 to the plasma membrane in vascular endothelial cells. *J. Physiol. Sci* **2020**, *70* (1), 44.
- (16) Spigoni, V.; Mena, P.; Cito, M.; Fantuzzi, F.; Bonadonna, R. C.; Brighenti, F.; Dei Cas, A.; Del Rio, D. Effects on nitric oxide production of urolithins, gut-derived ellagitannin metabolites, in human aortic endothelial cells. *Molecules* **2016**, *21* (8), 1009.
- (17) Song, W.; Yuan, Y.; Tan, X.; Gu, Y.; Zeng, J.; Song, W.; Xin, Z.; Fang, D.; Guan, R. Icariside II induces rapid phosphorylation of endothelial nitric oxide synthase via multiple signaling pathways. *PeerJ* **2022**, *10*, No. e14192.
- (18) Förstermann, U.; Sessa, W. C. Nitric oxide synthases: regulation and function. *Eur. Heart J* **2012**, *33* (7), 829–837.
- (19) Kolluru, G. K.; Siamwala, J. H.; Chatterjee, S. eNOS phosphorylation in health and disease. *Biochimie* **2010**, *92* (9), 1186–1198.
- (20) Sessa, W. C. Molecular control of blood flow and angiogenesis: role of nitric oxide. *J. Thromb. Haemost* **2009**, *7*, 35–37.
- (21) Reckzeh, E. S.; Waldmann, H. Small-molecule inhibition of glucose transporters GLUT-1–4. *ChemBiochem* **2020**, *21* (1–2), 45–52.
- (22) Morita, T.; Akiyoshi, T.; Sato, R.; Uekusa, Y.; Katayama, K.; Yajima, K.; Imaoka, A.; Sugimoto, Y.; Kiuchi, F.; Ohtani, H. Citrus fruit-derived flavanone glycoside narirutin is a novel potent inhibitor of organic anion-transporting polypeptides. *J. Agric. Food Chem* **2020**, *68* (48), 14182–14191.
- (23) Araki, N.; Morita, T.; Akiyoshi, T.; Kataoka, H.; Yajima, K.; Katayama, K.; Imaoka, A.; Ohtani, H. Comparison of the inhibitory properties of the fruit component naringenin and its glycosides against OATP1A2 genetic variants. *Drug Metab. Pharmacokinet* **2022**, *46*, 100464.
- (24) Yamaguchi, A.; Mukai, Y.; Sakuma, T.; Narumi, K.; Furugen, A.; Yamada, Y.; Kobayashi, M. Monocarboxylate transporter 4 involves in energy metabolism and drug sensitivity in hypoxia. *Sci. Rep* **2023**, *13* (1), 1501.
- (25) Gao, G.; Nakamura, S.; Asaba, S.; Miyata, Y.; Nakayama, H.; Matsui, T. Hesperidin preferentially stimulates transient receptor potential vanilloid 1, leading to NO production and mas receptor expression in human umbilical vein endothelial cells. *J. Agric. Food Chem* **2022**, *70* (36), 11290–11300.
- (26) Kimura, O.; Fujii, Y.; Haraguchi, K.; Kato, Y.; Ohta, C.; Koga, N.; Endo, T. Uptake of perfluorooctanoic acid by Caco-2 cells: Involvement of organic anion transporting polypeptides. *Toxicol. Lett* **2017**, *277*, 18–23.
- (27) Meng, X. L.; Guo, Y. L.; Huang, H. Y. The transport mechanism of monocarboxylate transporter on spinosin in Caco-2 cells. *Saudi Pharm. J* **2016**, *24* (3), 286–291.
- (28) Zhou, Y.; Hu, W.; Zhang, X.; Wang, Y.; Zhuang, W.; Li, F.; Li, Q. Cellular uptake and transport characteristics of FL118 derivatives in Caco-2 cell monolayers. *Chem. Pharm. Bull* **2021**, *69* (11), 1054–1060.
- (29) Serreli, G.; Le Sayec, M.; Thou, E.; Lacour, C.; Diotallevi, C.; Dhunna, M. A.; Deiana, M.; Spencer, J. P.; Corona, G. Ferulic acid derivatives and avenanthramides modulate endothelial function through maintenance of nitric oxide balance in HUVEC cells. *Nutrients* **2021**, *13* (6), 2026.
- (30) Greif, D. M.; Sacks, D. B.; Michel, T. Calmodulin phosphorylation and modulation of endothelial nitric oxide synthase catalysis. *Proc. Natl. Acad. Sci. U.S.A* **2004**, *101* (5), 1165–1170.
- (31) Tran, Q. K.; Ohashi, K.; Watanabe, H. Calcium signaling in endothelial cells. *Cardiovasc. Res* **2000**, *48* (1), 13–22.

(32) Yamada, N.; Makino, Y.; Clark, R. A.; Pearson, D. W.; Mattei, M. G.; Guenet, J. L.; Ohama, E.; Fujino, I.; Miyawaki, A.; Furuichi, T.; Mikoshiba, K. Human inositol 1, 4, 5-trisphosphate type-1 receptor, InsP3R1: Structure, function, regulation of expression and chromosomal localization. *Biochem. J* **1994**, *302* (3), 781–790.

(33) Lee, Y.; Nakano, A.; Nakamura, S.; Sakai, K.; Tanaka, M.; Sanematsu, K.; Shigemura, N.; Matsui, T. *In vitro* and *in silico* characterization of adiponectin-receptor agonist dipeptides. *Npj Sci Food* **2021**, *5* (1), 29.

(34) Jin, S. W.; Choi, C. Y.; Hwang, Y. P.; Kim, H. G.; Kim, S. J.; Chung, Y. C.; Lee, K. J.; Jeong, T. C.; Jeong, H. G. Betulinic acid increases eNOS phosphorylation and NO synthesis via the calcium-signaling pathway. *J. Agric. Food Chem* **2016**, *64* (4), 785–791.

(35) Warner, E. F.; Zhang, Q.; Raheem, K. S.; O'Hagan, D.; O'Connell, M. A.; Kay, C. D. Common phenolic metabolites of flavonoids, but not their unmetabolized precursors, reduce the secretion of vascular cellular adhesion molecules by human endothelial cells. *J. Nutr* **2016**, *146* (3), 465–473.

(36) Álvarez-Cilleros, D.; Ramos, S.; Goya, L.; Martín, M. A. Colonic metabolites from flavanols stimulate nitric oxide production in human endothelial cells and protect against oxidative stress-induced toxicity and endothelial dysfunction. *Food Chem. Toxicol* **2018**, *115*, 88–97.

(37) Houghton, M.; Kerimi, A.; Mouly, V.; Tumova, S.; Williamson, G. Gut microbiome catabolites as novel modulators of muscle cell glucose metabolism. *Faseb J* **2019**, *33* (2), 1887–1898.

(38) Tumova, S.; Kerimi, A.; Porter, K. E.; Williamson, G. Transendothelial glucose transport is not restricted by extracellular hyperglycaemia. *Vasc.Pharmacol* **2016**, *87*, 219–229.

(39) Wong, C. C.; Akiyama, Y.; Abe, T.; Lippiat, J. D.; Orfila, C.; Williamson, G. Carrier-mediated transport of quercetin conjugates: Involvement of organic anion transporters and organic anion transporting polypeptides. *Biochem. Pharmacol* **2012**, *84* (4), 564–570.

(40) Glaeser, H.; Bujok, K.; Schmidt, I.; Fromm, M. F.; Mandery, K. Organic anion transporting polypeptides and organic cation transporter 1 contribute to the cellular uptake of the flavonoid quercetin. *Naunyn-Schmiedeberg's Arch. Pharmacol* **2014**, *387* (9), 883–891.

(41) Riha, J.; Brenner, S.; Böhmendorfer, M.; Giessrigl, B.; Pignitter, M.; Schueller, K.; Thalhammer, T.; Stieger, B.; Somoza, V.; Szekeres, T.; Jäger, W. Resveratrol and its major sulfated conjugates are substrates of organic anion transporting polypeptides (OATPs): Impact on growth of ZR-75-1 breast cancer cells. *Mol. Nutr. Food Res* **2014**, *58* (9), 1830–1842.

(42) Konishi, Y.; Shimizu, M. Transepithelial transport of ferulic acid by monocarboxylic acid transporter in Caco-2 cell monolayers. *Biosci., Biotechnol., Biochem* **2003**, *67* (4), 856–862.

(43) Zhao, Y.; Vanhoutte, P. M.; Leung, S. W. Vascular nitric oxide: Beyond eNOS. *J. Pharmacol. Sci* **2015**, *129* (2), 83–94.

(44) Kuchan, M. J.; Frangos, J. A. Role of calcium and calmodulin in flow-induced nitric oxide production in endothelial cells. *Am. J. Physiol. Cell Physiol* **1994**, *266* (3), C628–C636.

(45) Dimmeler, S.; Fleming, I.; Fisslthaler, B.; Hermann, C.; Busse, R.; Zeiher, A. M. Activation of nitric oxide synthase in endothelial cells by Akt-dependent phosphorylation. *Nature* **1999**, *399* (6736), 601–605.